Visualization of MeV ion impacts in Si using scanning capacitance microscopy

Lasse Vines,* Edouard Monakhov,[1] Bengt G. Svensson,[1] Jens Jensen,[2] Anders Hallén,[3] and Andrej Yu. Kuznetsov[1]
[1]*Department of Physics/Physical Electronics, University of Oslo, P.O. Box 1048 Blindern, N-0316 Oslo, Norway*
[2]*Division of Ion Physics, Uppsala University, Box 534, SE-751 21 Uppsala, Sweden*
[3]*Department of Microelectronics and IT, Laboratory of Material and Semiconductor Physics, Royal Institute of Technology, Box Electrum 226, SE-164 40 Kista, Sweden*
(Received 21 October 2005; revised manuscript received 28 December 2005; published 14 February 2006)

Scanning capacitance microscopy (SCM) of 3 MeV Au^{2+} ion implanted Si have been performed for doses between 2×10^8 and 5×10^9 cm^{-2}. The measurements show a random pattern of reduced SCM signal (charge trapping) correlated with the ion impacts. These features have a lateral dimension of 150–600 nm and reveal a pronounced dose dependence. It is argued that the Fermi level near the impacts and along the ion tracks is modified (pinned) due to deep acceptor states formed by the penetrating ions. Substantial evidence for this argument is provided by SCM images obtained at different temperatures, where a strong correlation is revealed between the probing frequency and the emission rate of the single negative acceptor level of divacancy. To the best of our knowledge, this is a direct observation of signatures for individual ion impacts in Si by an electrical scanning technique.

DOI: 10.1103/PhysRevB.73.085312 PACS number(s): 61.72.Tt, 61.72.Bb, 71.55.Cn

I. INTRODUCTION

It has recently been suggested[1] that electrically active defects produced in Si along a heavy ion track can result in a pinning of the Fermi level to a dominant deep level such as the divacancy (V_2). This occurs within a region of <100 nm around an ion track and results in formation of a nanosized channel with a modified Fermi level embedded in bulk Si. The interpretation was based on deep level transient spectroscopy (DLTS) studies, where the intensity of the doubly negative charge state of the divacancy $[V_2(=/-)]$ peak is lower compared with that of the singly negative charge state of the divacancy $[V_2(-/0)]$. This has been attributed to a highly localized distribution of the defects along the ion tracks, which results in trapping of the carriers at $V_2(-/0)$ and incomplete occupancy of $V_2(=/-)$. Such nanochannels might act as electronic nanowires due to the local Fermi level modification that induces a bending of the electronic bands around the ion track. The technological advantage of such nanochannels is that, unlike the "traditional" nanowires, the ion-induced nanochannels are readily embedded into the Si crystal, a semiconductor in contrast to an oxide, by conventional ion implantation. Furthermore, a similar approach can also be used to manufacture nanodots with a modified Fermi level in layered structures consisting, e.g., of the same material having different doping or impurity concentrations. However, there are practically no direct ion track observations, or better to say visualization, reported in elemental semiconductors implanted with single MeV-ions. On the other hand there have been a number of such studies reported on ion tracks in compound semiconductors,[2–5] insulators,[6,7] metallic alloys,[8] ceramics,[9] and superconductors.[10] One possible explanation for that is a much more efficient annihilation of primary defects in the collision cascades that takes place in, e.g., Si so that traditional techniques measuring topographically or structurally related signals are not sensitive enough for the ion track visualization. Only tracers of low energy (10–120 keV) impacts of heavy ions[11] or clusters[12] have been visualized and studied using topographically related techniques in Si.

One modern technique of visualization of electrical characteristics of semiconductors is scanning capacitance microscopy (SCM),[13] which is based on atomic force microscopy (AFM) using a conductive tip, measuring the change in capacitance over a sample simultaneously with the topography by utilizing an ultrahigh frequency resonance capacitance sensor. SCM has been successfully applied to observe, e.g., quantum wells in InGaAs/InP[14] and ultranarrow doping profiles in Si.[15] Obviously, for detecting the electrically modified nanochannels one must obtain a proper balance between the original carrier concentration in the sample and the implantation characteristics such as ion, energy, and dose, which determine the charge trapping in the damaged regions. For example, the energy must be low enough such that the elastic energy deposition is significant, i.e., the generated stable point defects after impact per ion and Å is comparable to the doping, but still high enough to produce an extended channel. In this study, we report on the dose and temperature dependence of traces of 3 MeV Au^{2+} ion implants into *n*-type Si using SCM.

II. EXPERIMENTAL

Samples were cut from *n*-type Czochralski (Cz) Si(100) wafers doped with phosphorus to $\sim10^{16}$ cm^{-3}. The samples were implanted at room temperature (RT) with 3 MeV Au^{2+} ions using three different doses, 2×10^8, 8×10^8, and 5×10^9 cm^{-2}, and the implants were performed at the Tandem Laboratory, Uppsala University. The doses were chosen based on TRIM simulations[16] and estimates of the instantaneous annihilation rate.[17] Additionally, one sample was dipped in hydrofluoric acid (HF) and immediately loaded into the implantation chamber, aiming to implant the sample without (or minimizing) the native oxide thickness. A control

 ©2006 The American Physical Society

experiment was carried out at a lower energy, a 1.4 MeV Au^{2+} implantation with a dose of 5×10^{9} cm^{-2}, to bring the peak damage region closer to the surface. After the ion implantation the samples were mounted on the sample stage of an atomic force microscope (AFM) equipped with a Peltier element for measurements in the range of 8–50 °C and having the temperature accuracy of ±3 °C. The mounting was made using conductive silver paste together with a wire connecting the sample and the stage electrically. The temperature was measured by a thermocouple mounted on the Peltier element in direct vicinity to the sample.

The SCM measurements were undertaken employing a Nanoscope Dimension 3100 microscope from Veeco Instruments equipped with capacitance measurement electronics. Commercial metal (Ti-Pt) coated and etched silicon tips (purchased from MicroMasch) with a tip curvature radius less than 40 nm were used for operating in contact mode. The capacitance measurements were carried out in a differential capacitance-voltage (dC/dV) mode with an ac modulation frequency of 60 kHz, ac modulation voltage at 1 V, and the dc bias at 0 V. All observations were obtained in a plan view using different scan areas. In the SCM measurements the tip and the sample form a metal-insulator-semiconductor (MIS) capacitor with the surface native oxide acting as a thin insulating layer. If the amplitude of the ac voltage (dV) is kept constant, the magnitude of capacitance variation (dC) is in general a nonlinear decreasing function of the charge concentration. This implies that in two-dimensional black and white SCM diagrams the darker color corresponds to regions containing more charges. Quantitative SCM measurements have been demonstrated,[18] but SCM has traditionally been used for qualitative imaging. This is also the focus for the experiments described here, and only raw SCM data are therefore shown. The spatial feature size in the measurements is determined by the depletion region in the MIS structure.[19] Simultaneously to SCM, the topography of the sample was measured by a feedback loop keeping a constant cantilever deflection (force mode AFM), in order to exclude the topography influence on the measured capacitance variations.

In addition, DLTS measurements were employed in order to measure the average defect concentrations and correlate the present SCM data with previously reported DLTS data.[1] Samples for the DLTS measurements were cleaned after irradiation, including a final dip in HF, before loading into a vacuum chamber for metal deposition. Schottky barrier contacts with a thickness of ≈300 nm were deposited at RT using thermal evaporation of gold through a metal mask with circular openings of 1 mm in diameter. The DLTS setup used is a refined version of the one described in Ref. 20.

III. RESULTS AND DISCUSSION

A. Defect production

Figure 1 shows the results of TRIM simulations for a single impact of a 3 MeV Au^{2+} ion into Si. One can observe that the atomic displacements are confined to relatively narrow regions (≲30 nm in diameter). The average vacancy generation rate in the near surface region (≲3000 Å) is about 2.8 per ion per Å, although the defect distribution is naturally nonuniform, with high density around the secondary cascades. From Fig. 1(B) one can estimate an average primary defect concentration in the damaged regions to be in the range of 10^{19} cm^{-3}, assuming an ion track diameter of 30 nm. However, it is well established[17] that only a few percent of the generated vacancies and interstitials escape recombination, which suggests a local defect concentration on the order of 10^{17} cm^{-3}. Interestingly, this concentration is above a threshold level for macroscopic changes of electronic properties in Si in accordance with Ref. 21.

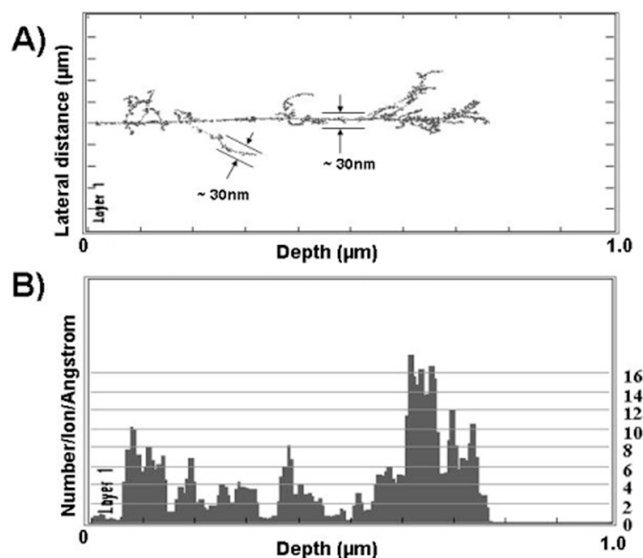

FIG. 1. A TRIM simulation of a 3 MeV Au^{2+} ion impact in Si. The figure shows (A) the full cascade of the Au^{2+} ion and several secondary cascades, and (B) the vacancy distribution. The arrow indicates the dimensions of the nanosized defect channels.

The local defect concentration based on TRIM simulations is in accordance with results from DLTS measurements. For example, an average bulk concentration of 2×10^{14} cm^{-3} is detected by DLTS for V_2 in the sample implanted with a dose of 2×10^{8} cm^{-2}. Indeed, this results in a local concentration of $\sim10^{17}$ cm^{-3} for V_2 along the ion tracks assuming that the majority of the defects are concentrated along the ion tracks with an average size of ~30 nm. This analysis suggests a highly modified local charge concentration around the ion trajectory, motivating the visualization of the ion-induced channels using SCM.

B. AFM and SCM measurements

Figures 2(A)–2(D) show the results of SCM measurements performed in a plan view with a scan size of 4×4 μm for samples implanted with doses 5×10^{9}, 8×10^{8}, and 2×10^{8} cm^{-2} as well as for the unimplanted sample, respectively. In the samples implanted with the two highest doses, Figs. 2(A) and 2(B), a random pattern of dark regions with diameter of ~150–600 nm is observed. As discussed previously, the darker regions in SCM images are readily interpreted as signatures for an increase in charge concentration in the corresponding regions of the samples as compared with the original substrate conditions.

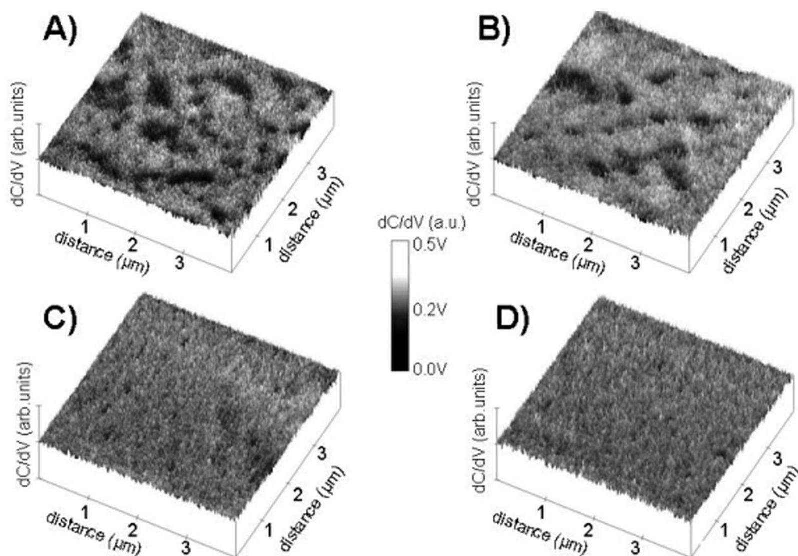

FIG. 2. SCM images of Si samples implanted with 3 MeV Au^{2+} ions with dose 5×10^{9} cm^{-2} (A), 8×10^{8} cm^{-2} (B) and 2×10^{8} cm^{-2} (C), as well as a nonimplanted sample (D).

The topography of the samples were measured simultaneously and are shown for the high dose and references sample in Figs. 3(A) and 3(B), respectively. The roughness is defined by

$$R_q = \sqrt{\frac{\sum_{i=1}^{N} (Z_i - Z_{ave})^2}{N}},$$

where Z_i is the measured height in the image, Z_{ave} is the average height, and N is the number of pixels in the image. The surface roughness of the implanted and reference samples are similar, 0.20 and 0.18 ± 0.03, respectively, with some minor topographical features in both the reference sample and the implanted sample. These features are presumably contamination of the surfaces, and represent typical observation, although the type of contamination is not specific for the implanted or reference sample. The contaminations in the AFM images in Fig. 3 are shown intentionally to illustrate if and how topographical features influence the measurements. Overall, the change in surface roughness is negligible, in contrast to the AFM studies using higher energies and doses,[22] and the SCM pattern observed in Figs. 2(A) and 2(B) cannot be explained by these topographical features, concluding that the pattern arises from electronic modification of the samples.

The fact that the regions with increased charge concentration appear in the implanted samples and not in the reference sample shows that the increased charge concentration in Figs. 2(A) and 2(B) is due to the ion implantation process. Potentially, there are two possibilities causing the charge accumulation; (i) implantation induced deep acceptor states in the bulk Si as discussed above or (ii) implantation induced charges in the native oxide. To verify that the measured increase in charge is from the bulk Si, an additional sample was implanted where the native oxide was removed by a dip in HF immediately before loading into the implantation chamber. The SCM pattern was observed on this sample as well, supporting hypothesis (i) as the primary cause of the measured increase in charge in Fig. 2. Interestingly, the spatial feature size of the dark regions in the SCM measurements are larger than the expected size of the nanochannels according to TRIM. However, as discussed above, the feature size in Fig. 2 depends also on the size of the depletion region in the MIS structure, ~300 nm for the given experimental conditions, which is consistent with the observations in Fig. 2. This also supports hypothesis (i) since charges in the native oxide would give a spatial feature size in the range of the ion track.

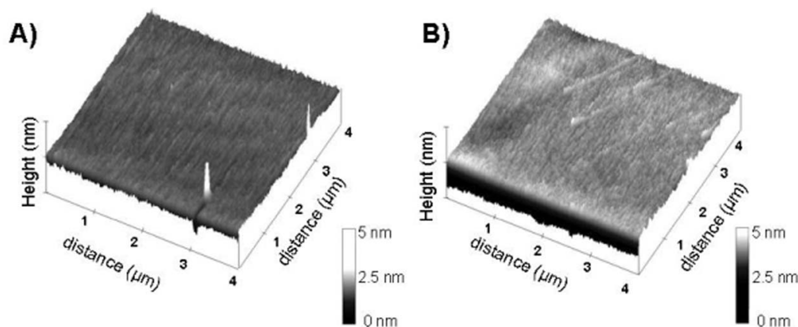

FIG. 3. Topography of (A) Si sample implanted with 3 MeV Au^{2+} ions with dose 5×10^{9} cm^{-2}, and (B) a reference sample.

C. Dose and energy dependence

The number of regions with a modified charge concentration in Fig. 2 does not show a linear dose-dependence. The samples implanted with the highest and medium doses [Figs. 2(A) and 2(B)] exhibit ~60 and 20 regions with increased charge concentration, respectively. The sample implanted with the lowest dose shows a uniform dC/dV contrast similar to that observed in the virgin sample. The average number of features measured over five images taken at different occasions, the feature size measured at the longest side and its standard deviation for the high dose sample were found to be 3.36×10^{8} cm^{-2}, 323 nm, and 138 nm, respectively, while the corresponding numbers for the medium dose sample are 1.35×10^{8} cm^{-2}, 363 nm, and 142 nm. The feature size was determined by visual inspection. The number of the dark regions in Figs. 2(A) and 2(B) is only a fraction of the number of ion impacts for corresponding doses, 7 and 17% for the high and medium dose sample, respectively. There are at least two possible explanations for such behavior. Firstly, the ion induced defect density varies considerably with the depth, as seen in Fig. 1(B). Since the probed volume during SCM measurements is within ~300 nm from the surface only a part of the ion track is covered. It is also well known[1] that the annihilation of defects is stronger in the near surface region than further into the bulk Si. Thus, only a fraction of the nanochannels will, due to the statistical nature of the process, have sufficient defect density to exceed the measurement sensitivity. Secondly, a single ion track may not give sufficient dC/dV contrast, since the channel occupies only a fraction of the totally probed sample volume. At the same time, a superposition of several nearby tracks can result in a capacitance change above the detection limit. For low doses the ion tracks will, on average, be well separated and only one track will be within the depletion region at a time. As the dose increases, the average distance between the channels decreases and several tracks can occur within the depletion region, resulting in a larger change in the capacitance compared to the bulk region.

Interestingly, one may estimate a threshold dose for several ion impacts to be within the depletion region of $\sim 4\times 10^{8}$ cm^{-2} using current substrate conditions. This is in accordance with the observation of the dose dependence, where the features are not observed for the sample implanted with the lowest dose, 2×10^{8} cm^{-2}. In addition, for the two highest doses the depletion region is larger than the average distance between the ion impacts, which will result in a nonlinear dose-dependence of the number of observed features. This argument favors the second explanation as the primary cause of the observed features.

As discussed above, probing only one probe a fraction of the ion track, interesting progress may be made by removing the surface layer by layer, so that measurements can be carried out as a function of depth. However, since the charge distribution in the sample is nonuniform due to the ion impacts, as proposed in Ref. 1, internal electric fields arise and influence the etching rate. Indeed, our wet etching results in a roughening of the sample, making the SCM measurements difficult to interpret. However, instead of etching the sample to probe the region closer to the damage peak at the end of the ion track, one could implant samples at lower energies.

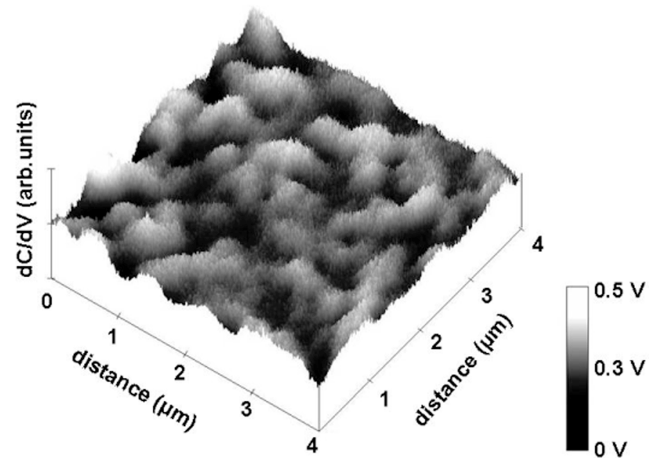

FIG. 4. An SCM image of Si samples implanted with 1.4 MeV Au^{2+} ions with a dose of 5×10^{9} cm^{-2}.

Figure 4 shows an image of a 1.4 MeV Au^{2+} implanted sample with a dose of 5×10^{9} cm^{-2}. The sample exhibits a pattern similar to that in Fig. 2(A), but, as anticipated, the contrast is more distinguished here. Consequently, the increased charge concentration close to the damage peak will result in an increased dC/dV contrast, but not change the "morphology" of the pattern in the dC/dV images.

D. Temperature dependence

Investigating the temperature dependence one must take into account the specifics of the SCM measurements (i.e., frequency, bias, etc.) and the fact that the interaction of charge carriers with electrically active defects depends strongly on the position of the levels in the band gap. The emission rate of the electrons to the conduction band, e_n, follows the Shokley-Read-Hall statistics, and is given by $e_n(T)=\nu_{\mathrm{th}}\gamma\sigma_n N_C \exp(-\Delta G/kT)$,[23] where ν_{th} is the average electron velocity, γ is the degeneracy of the defect level, σ_n is the electron capture cross section, N_C is the effective density of states in the conduction band, ΔG is the ionization free energy, k is Boltzmann constant, and T is the absolute temperature. If a boxlike pulse is applied to the sample the number of filled states at a time after removing the pulse will be given by $N_T(filled)=N_T \exp[-e_n(T)t]$ with a characteristic time constant $\tau=1/e_n$. For the $V_2(-/0)$ state located at ~0.43 eV below the conduction band edge, the corresponding characteristic frequency $1/\tau$ is in the range of 10 kHz at RT and 100 kHz at 50 °C.[24] Thus, having the probing SCM frequency at 60 kHz, which is the measurement condition for the samples in Fig. 2, the thermal emission rate will not be sufficient for the electrons trapped at the $V_2(-/0)$ levels to interact with the conduction band at RT. On the other hand, at elevated temperatures the emission rate can exceed the probing frequency reducing the charge concentration difference between the matrix and the damaged regions around ion tracks.

Figures 5(A)–5(C) show SCM results for the sample implanted with the dose of 5×10^{9} cm^{-2} as measured at three

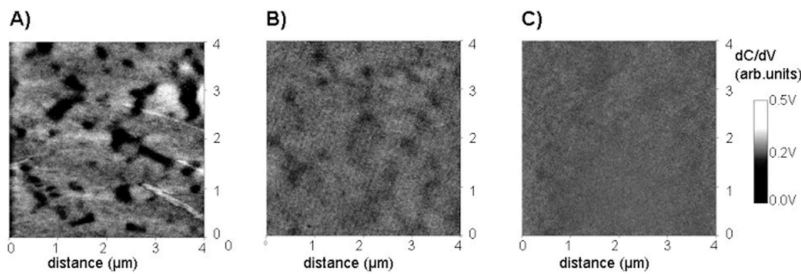

FIG. 5. SCM images of Si implanted with 3 MeV Au^{2+} ions with a dose of 5×10^9 cm^{-2} as measured at (A) 8° C, (B) 35° C, and (C) 50° C.

different temperatures, 8, 35, and 50° C, respectively, and both V_2 and VO are known to be stable at the measurement temperatures.[17] The measurements at RT [Fig. 2(A)] and below [Fig. 5(A)] show a pattern with an increased charge concentration. In this case, the electrons are trapped at the $V_2(-/0)$ level increasing the local charge concentration in the impact regions. However, at elevated temperatures [Figs. 5(B) and 5(C)] the electrons are released from this level with a sufficient rate to respond to the measurement frequency, resulting in the reduced contrast of the SCM features.

IV. CONCLUSIONS

In conclusion, a direct and unique observation of MeV ion impacts in Si is made employing SCM imaging. The SCM images display a random pattern of the reduced dC/dV signal (charge trapping) and a pronounced dose-dependence is revealed; this is discussed in terms of the defect distribution along the ion track and/or overlapping of the individual ion tracks within the depletion region created by the SCM tip. It is argued that the local Fermi level along the ion tracks is pinned by deep acceptor states, primarily $V_2(-/0)$, forming nanochannels with modified electronic properties. A strong temperature dependence for the contrast of the observed dC/dV pattern is revealed correlating with the probing frequency and the divacancy acceptor level position.

ACKNOWLEDGMENT

This work was supported by the Norwegian Research Council through the NanoMat program and additional support was provided by NordForsk via the NOCDAD network.

*Electronic address: Lasse.Vines@fys.uio.no

[1] E. V. Monakhov, J. Wong-Leung, A. Yu. Kuznetsov, C. Jagadish, and B. G. Svensson, Phys. Rev. B **65**, 245201 (2002).
[2] A. Hida, A. Iwase, Y. Mera, T. Kambara, and K. Maeda, Nucl. Instrum. Methods Phys. Res. B **209**, 140 (2003).
[3] F. Komarov, P. Gaiduk, and A. Kamarou, Vacuum **63**, 657 (2001).
[4] P. I. Gaiduk, A. Nylandsted Larsen, J. Lundsgaard Hansen, C. Trautmann, and M. Toulemonde, Appl. Phys. Lett. **83**, 1746 (2003).
[5] J. Vetter, R. Scholz, D. Dobrev, and L. Nistor, Nucl. Instrum. Methods Phys. Res. B **141**, 747 (1998).
[6] J. Krauser, J.-H. Zollondz, A. Weidinger, and C. Trautmann, J. Appl. Phys. **94**, 1959 (2003).
[7] C. Houpert, F. Studer, D. Groult, and M. Toulemonde, Nucl. Instrum. Methods Phys. Res. B **39**, 720 (1989).
[8] A. Audouard, R. Mamy, M. Toulemonde, G. Szenes, and L. Thome, Europhys. Lett. **40**, 527 (1997).
[9] C. Müller, M. Cranney, A. El-Said, N. Ishikawa, A. Iwase, M. Lang, and R. Neumann, Nucl. Instrum. Methods Phys. Res. B **191**, 246 (2002).
[10] J. Wiesner, C. Træholt, J.-G. Wen, H.-W. Zandbergen, G. Wirth, and H. Fuess, Physica C **268**, 161 (1996).
[11] L. M. Howe and M. H. Rainville, Nucl. Instrum. Methods **182/183**, 143 (1981).
[12] V. N. Popok, S. V. Prasalovich, and E. E. B. Campbell, Vacuum **76**, 265 (2004).
[13] C. C. Williams, Annu. Rev. Mater. Sci. **29**, 471 (1999).
[14] K. Maknys, O. Douhéret, and S. Anand, Appl. Phys. Lett. **83**, 4205 (2003).
[15] F. Giannazzo, D. Goghero, V. Raineri, S. Mirabella, and F. Priolo, Appl. Phys. Lett. **83**, 2659 (2003).
[16] J. F. Ziegler, J. P. Biersack, and U. Littmark, *The Stopping and Range of Ions in Solids* (Pergamon, New York, 1985).
[17] B. G. Svensson, C. Jagadish, A. Hallén, and J. Lalita, Phys. Rev. B **55**, 10498 (1997).
[18] F. Giannazzo, L. Calcagno, V. Raineri, L. Ciampolini, M. Ciappa, and E. Napolitani, Appl. Phys. Lett. **79**, 1211 (2001).
[19] H. E. Ruda and A. Shik, Phys. Rev. B **71**, 075316 (2005).
[20] B. G. Svensson, K.-H. Rydén, and B. M. S. Lewerentz, J. Appl. Phys. **66**, 1699 (1989).
[21] M. Levalois, P. Bogdanski, and M. Toulemonde, Nucl. Instrum. Methods Phys. Res. B **63**, 14 (1992).
[22] P. Srivastava, V. Ganesan, and O. Sinha, Nucl. Instrum. Methods Phys. Res. B **187**, 220 (2002).
[23] W. Shockley and W. T. Read, Phys. Rev. **87**, 835 (1952).
[24] Note, that VO and $V_2(=/-)$ may also contribute to the charge trapping but less efficiently because of a more shallow location in the band gap comparing with $V_2(-/0)$.